nated to a surface Al, providing a mechanism for the interchange of $O_s$ and $O_{ads}$. These results also provide evidence for incipient $Al(OH)_3$ formation on the surface. The ultimate structure of the heavily hydrated surface is clearly very complicated and may depend strongly on sample history. It is possible that the $Al(OH)_3$ species can be removed completely (perhaps starting near steps or other defects), leaving a less reactive surface that is completely $O_sH$-terminated, which is similar to the known surfaces of aluminum hydroxides (*1*).

An idealized model for fully hydroxylated $\alpha$-$Al_2O_3$(0001) (*28*) replaces each surface Al with three H atoms (Fig. 5A), yielding a coverage >15 OH per square nanometer. Room-temperature MD simulations of this model revealed a complex dynamic structure (Fig. 5B), with one out of every three OH groups, on average, lying parallel to the surface because of in-plane hydrogen bonding. Calculated O–H vibrational spectra (*25*) yielded two broad peaks at ~3470 and 3650 $cm^{-1}$, with the peak at ~3470 $cm^{-1}$ corresponding to in-plane OH groups. The peak at ~3650 $cm^{-1}$ is close to the single peak (3720 to 3733 $cm^{-1}$) that is observed in most measurements on hydroxylated $\alpha$-$Al_2O_3$(0001) (*29*) and to the range that is generally assigned to bridging OH groups (*2*, *26*). The peak at ~3470 $cm^{-1}$ is red-shifted by hydrogen bonding and is generally not seen in single-crystal experiments, perhaps because of selection rules or because it is too broad. Our finding of two peaks split by 200 $cm^{-1}$ contradicts all previous classifications of OH vibrations (and subsequent cluster modeling) (*2*) on aluminas, which assume that all OH groups with the same coordination of O and neighboring Al have the same frequency. By this criterion, all of the surface OH groups in Fig. 5 are equivalent; however, their stretch frequencies clearly depend also on longer range environmental effects.

The present investigation of $\alpha$-$Al_2O_3$(0001) has elucidated several aspects of the complex interactions of $H_2O$ with an alumina surface, especially the dynamics of dissociation reactions at low and high coverages. On the basis of these results, a consistent interpretation of a diverse set of experimental data on hydroxylated alumina surfaces begins to emerge.

**References and Notes**


1. K. Wefers and C. Misra, *Alcoa Tech. Pap. 19 (revised)* (Alcoa Laboratories, St. Louis, MO, 1987).
2. H. Knözinger and P. Ratnasamy, *Catal. Rev. Sci. Eng.* **17**, 31 (1978).
3. M. Gautier *et al.*, *J. Am. Ceram. Soc.* **77**, 323 (1994).
4. P. de Sainte Claire, K. C. Hass, W. F. Schneider, W. L. Hase, *J. Chem. Phys.* **106**, 7331 (1997).
5. G. N. Robinson, Q. Dai, A. Freedman, *J. Phys. Chem. B* **101**, 4940 (1997).
6. R. Car and M. Parrinello, *Phys. Rev. Lett.* **55**, 2471 (1985).
7. The gradient-corrected exchange-correlation [Bernstein, Lee, Yang, and Primakoff (BLYP)] functional used here is from A. D. Becke [*Phys. Rev. A* **38**, 3098 (1988)] and C. Lee, W. Yang, and R. Parr [*Phys. Rev. B* **37**, 785 (1988)]. Norm-conserving numerical pseudopotentials were generated for Al and O with the procedure of N. Troullier and J. L. Martins [*ibid.* **43**, 1993 (1991)], and a local analytic pseudopotential was derived for H. This is essentially a softened Coulomb potential with a core radius of 0.25 atomic units. Electron wave functions are expanded in a plane-wave basis set with an energy cutoff of 70 rydbergs (Ry). We used the Car-Parrinello Molecular Dynamics code in the parallelized 2.5 version (developed by J. Hutter and copyrighted by IBM, Armonk, NY). All calculations were performed on a 32-node IBM RS6000 SP at the IBM Watson Research Laboratory (Yorktown Heights, NY).
8. In the MD runs, a value of 400 au was used for the fictitious electron mass of the Car-Parrinello Lagrangian multipliers (*6*), and each hydrogen molecule was replaced by deuterium to improve the separation between electronic and ionic degrees of freedom. The time step in the Verlet algorithm for the integration of the equations of motions was ~0.1 fs.
9. The importance of chemical reaction dynamics in general has recently been highlighted in a special issue of *Science* [Reaction Dynamics, *Science* **279**, 1875–1895 (1998)].
10. A. Curioni *et al.*, *J. Am. Chem. Soc.* **119**, 7218 (1997).
11. V. E. Puchin *et al.*, *Surf. Sci.* **370**, 190 (1997); J. Ahn and J. W. Rabalais, *ibid.* **388**, 121 (1997).
12. See, for example, S. Blonski and S. H. Garofalini, *ibid.* **295**, 263 (1993).
13. See, for example, M. Causa, R. Dovesi, C. Pisani, C. Roetti, *ibid.* **215**, 259 (1989); I. Manassidis, A. De Vita, M. J. Gillan, *Surf. Sci. Lett.* **285**, L517 (1993); I. Frank, D. Marx, M. Parrinello, *J. Chem. Phys.* **104**, 8143 (1996).
14. J. M. McHale, A. Auroux, A. J. Perrotta, A. Navrotsky, *Science* **277**, 788 (1997). For earlier work, see P. A. Thiel and T. E. Madey, *Surf. Sci. Rep.* **7**, 211 (1987) and references therein.
15. J. M. Wittbrodt, W. L. Hase, H. B. Schlegel, *J. Phys. Chem. B* **102**, 6539 (1998).
16. K. C. Hass, W. F. Schneider, A. Curioni, W. Andreoni, in preparation.
17. Earlier calculations used much smaller supercells than the present work. Such studies were therefore limited in their ability to provide accurate adsorbate structures and energies and to study the $H_2O$ coverage dependence and phenomena such as collective effects and surface diffusion.
18. J. Goniakowski and M. J. Gillan, *Surf. Sci.* **350**, 145 (1996); P. J. D. Lindan, N. M. Harrison, J. M. Holdender, M. J. Gillan, *Chem. Phys. Lett.* **261**, 246 (1996); P. J. D. Lindan, N. M. Harrison, M. J. Gillan, *Phys. Rev. Lett.* **80**, 762 (1998).
19. W. Langel and M. Parrinello, *J. Chem. Phys.* **103**, 3240 (1995).
20. Lagrange multipliers were introduced to constrain the relevant H–$O_s$ distance, and the average constraint forces were determined from constant temperature simulations [S. Nosé, *J. Chem. Phys.* **81**, 511 (1984); W. G. Hoover, *Phys. Rev. A* **31**, 1695 (1985)] of at least 0.2 ps.
21. S. Scheiner, in *Proton Transfer in Hydrogen-Bonded Systems*, T. Bountis, Ed. (Plenum, New York, 1992), p. 29.
22. S. Blonski and S. H. Garofalini, *J. Phys. Chem.* **100**, 2201 (1996).
23. The temperature was not controlled but was increased slowly from ~100 to ~350 K. The system was then allowed to evolve for a time interval of >1 ps. The average temperature was 250 K.
24. D. E. Brown, D. J. Moffatt, R. A. Wolkow, *Science* **279**, 542 (1998).
25. Vibrational frequencies were estimated from the power spectra of the (partial) velocity-velocity autocorrelation functions and were rescaled to account for the fictitious electronic mass and the different mass used for the proton.
26. V. I. Lygin and I. S. Muzyka, *Russ. J. Phys. Chem.* **69**, 1829 (1995); A. Tsyganenko and P. Mardilovich, *J. Chem. Soc. Faraday Trans.* **92**, 4843 (1996).
27. B. A. Huggins and P. D. Ellis, *J. Am. Chem. Soc.* **114**, 2098 (1992).
28. M. A. Nygren, D. H. Gay, C. R. A. Catlow, *Surf. Sci.* **380**, 113 (1997).
29. C. Morterra, G. Ghiotti, E. Garrone, F. Boccuzzi, *J. Chem. Soc. Faraday Trans. 1* **72**, 2722 (1976); J. G. Chen, J. E. Crowell, J. T. Yates, *J. Chem. Phys.* **84**, 5906 (1986); V. Coustet and J. Jupille, *Surf. Sci.* **307**, 1161 (1994).


11 August 1998; accepted 3 September 1998

# Past Temperatures Directly from the Greenland Ice Sheet

**D. Dahl-Jensen,* K. Mosegaard, N. Gundestrup, G. D. Clow, S. J. Johnsen, A. W. Hansen, N. Balling**

**A Monte Carlo inverse method has been used on the temperature profiles measured down through the Greenland Ice Core Project (GRIP) borehole, at the summit of the Greenland Ice Sheet, and the Dye 3 borehole 865 kilometers farther south. The result is a 50,000-year-long temperature history at GRIP and a 7000-year history at Dye 3. The Last Glacial Maximum, the Climatic Optimum, the Medieval Warmth, the Little Ice Age, and a warm period at 1930 A.D. are resolved from the GRIP reconstruction with the amplitudes –23 kelvin, +2.5 kelvin, +1 kelvin, –1 kelvin, and +0.5 kelvin, respectively. The Dye 3 temperature is similar to the GRIP history but has an amplitude 1.5 times larger, indicating higher climatic variability there. The calculated terrestrial heat flow density from the GRIP inversion is 51.3 milliwatts per square meter.**

Measured temperatures down through an ice sheet relate directly to past surface temperature changes. Here, we use the measurements from two deep boreholes on the Greenland Ice Sheet to reconstruct past temperatures. The GRIP ice core (72.6°N, 37.6°W) was successfully recovered in 1992 (*1, 2*), and the 3028.6-m-deep liquid-filled borehole with a diameter of 13 cm was left undisturbed. Temperatures were then measured down through the borehole in 1993, 1994, and 1995 (*3, 4*). We used the measurements from 1995 (Fig. 1) (*4*), because there was no remaining evidence of disturbances from the drilling and

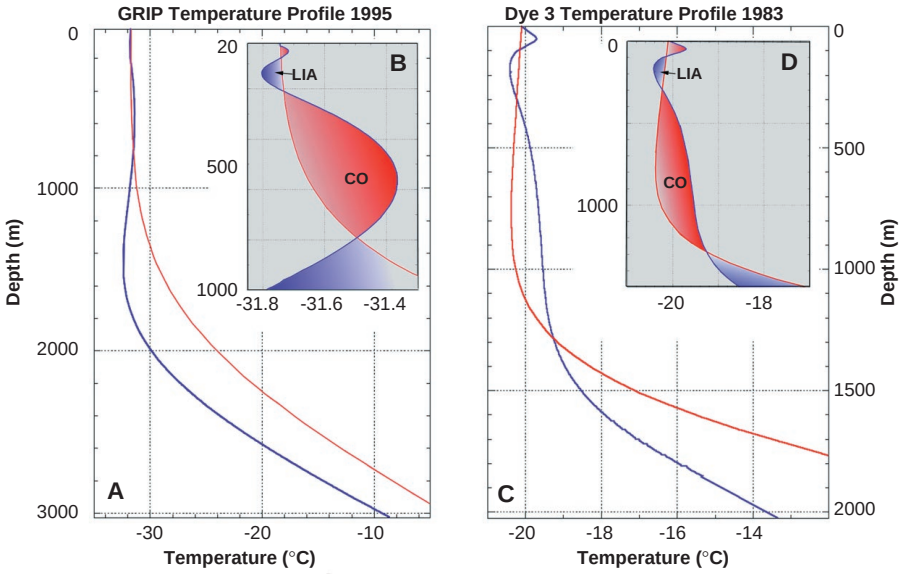


**Fig. 1.** The GRIP and Dye 3 temperature profiles [blue trace in (A) and (C)] are compared to temperature profiles [red trace in (A) and (C)] calculated under the condition that the present surface temperatures and accumulation rates have been unchanged back in time. (**A**) The GRIP temperature profile measured in 1995. The cold temperatures from the Glacial Period (115 to 11 ka) are seen as cold temperatures between 1200- to 2000-m depth. (**B**) The top 1000 m of the GRIP temperature profiles are enlarged so the Climatic Optimum (CO, 8 to 5 ka), the Little Ice Age (LIA, 1550 to 1850 A.D.), and the warmth around 1930 A.D. are indicated at the depths around 600, 140, and 60 m, respectively. (**C**) The Dye 3 temperature profile measured in 1983. Note the different shape of the temperature profiles when compared to GRIP and the different depth locations of the climate events. (**D**) The top 1500 m of the Dye 3 temperature profiles are enlarged so the CO, the LIA, and the warmth around 1930 A.D. are indicated at the depths around 800, 200, and 70 m, respectively.

the measurements were the most precise (±5 mK). Temperatures measured in a thermally equilibrated shallow borehole near the drill site are used for the top 40 m, because they are more reliable than the GRIP profile over this depth (*5*). The present mean annual surface temperature at the site is –31.70°C. The 2037-m-deep ice core from Dye 3 (65.2°N, 43.8°W) was recovered in 1981. We used temperature data from 1983 measurements with a precession of 30 mK (*6, 7*). The temperatures at the bedrock are –8.58°C at GRIP and –13.22°C at Dye 3. Calculations show that the basal temperatures have been well below the melting point throughout the past 100,000 years (*8*). Because there are still climate-induced temperature changes near the bedrock, we included 3 km of bedrock in the heat flow calculatin.

Past surface temperature changes are indicated from the shape of the temperature profiles (Fig. 1). We used a coupled heat- and ice-flow model to extract the climatic information from the measured temperature profiles. The temperatures down through the ice depend on the geothermal heat flow density (heat flux), the ice-flow pattern, and the past surface temperatures and accumulation rates. The past surface temperatures and the geothermal heat flow density are unknowns, whereas the past accumulation rates and ice-flow pattern are assumed to be coupled to the temperature history through relations found from ice-core studies (*9–11*). The total ice thickness is assumed to vary 200 m as described in (*9*). The coupled heat- and ice-flow equation is (*7, 9, 12*)

$$\rho c \frac{\partial T}{\partial t} = \nabla \cdot (K \nabla T) - \rho c \vec{v} \cdot \nabla T + f$$

where $T(x,z,t)$ is temperature, $t$ is time, $z$ is depth, $x$ is horizontal distance along the flow line, $\rho(z)$ is ice density, $K(T,\rho)$ the thermal conductivity, $c(T)$ is the specific heat capacity, and $f(z)$ is the heat production term. The ice velocities, $\vec{v}$ $(x,z,t)$, are calculated by an ice-flow model (*9, 13*). Model calculations to reproduce a present-day temperature profile through the ice sheet are started 450,000 years ago (ka) at GRIP (100 ka at Dye 3),

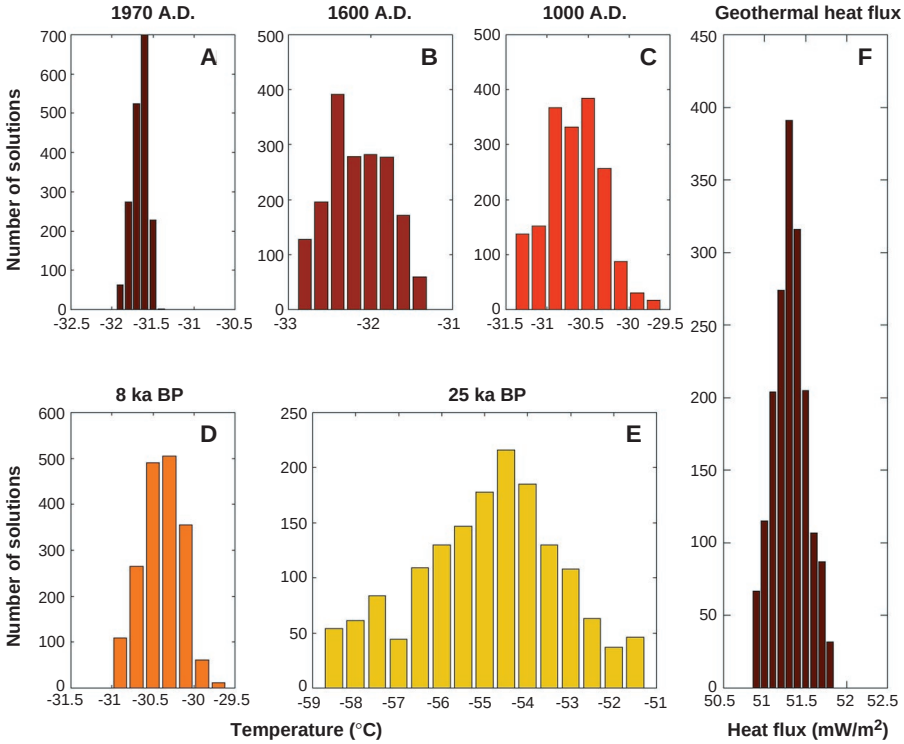


**Fig. 2.** (**A** through **E**) The probability distributions of the past surface temperatures at the Greenland Ice Sheet summit at selected times before present. They are constructed as histograms of the 2000 Monte Carlo sampled and accepted temperature histories (*17*). All temperature distributions are seen to have a zone with maximum values, the most likely values, which are assumed to be the reconstructed surface temperature at these times (*18*). (**F**) The probability distribution of the sampled geothermal heat flow densities. The most likely value is 51.3 mW/m$^2$.

D. Dahl-Jensen, K. Mosegaard, N. Gundestrup, S. J. Johnsen, A. W. Hansen, Niels Bohr Institute for Astronomy, Physics and Geophysics, Department of Geophysics, Juliane Maries Vej 30, DK-2100 Copenhagen OE, Denmark. G. D. Clow, USGS-Climate Program, Box 25046, MS 980, Denver Federal Center, Denver, CO 80225, USA. N. Balling, Department of Earth Sciences, Geophysical Laboratory, University of Aarhus, Finlandsgade 8, DK-8200 Aarhus N, Denmark.

*To whom correspondence should be addressed. E-mail: ddj@gfy.ku.dk

more than twice the time scale for thermal equilibrium of the ice-bedrock, so the unknown initial conditions are forgotten when generating the most recent 50,000-year temperature history (7000 years for Dye 3).

We developed a Monte Carlo method to fit the data and infer past climate. The Monte Carlo method tests randomly selected combinations of surface temperature histories and geothermal heat flow densities by using them as input to the coupled heat- and ice-flow model and considering the resulting degrees of fit between the reproduced and measured temperature profiles (*14–16*). Our results for each site are based on tests of $3.3 \times 10^6$ combinations of temperature histories and heat flow densities, of which 2000 solutions have been selected (*17*). The 2000 temperature histories and heat flow densities are sampled with a frequency proportional to their likelihood (*14, 15*), and all accepted solutions fit the observations within their limits of uncertainty.

Histograms of the sampled geothermal heat flow densities and of the temperature histories at each time before present can be made (for example, Fig. 2). The distributions in general show that there is a most likely value, a maximum, at all times, which we refer to as the temperature history (*18*). The distribution of accepted geothermal heat flow densities (Fig. 2F) has a median of 51.3 ± 0.2 mW/m$^2$, which is slightly higher than the heat flow density from Archean continental crust across the Baffin Bay in Canada. A few heat flow measurements have been made from the coast of Greenland (36 and 43 mW/m$^2$), but these are not corrected for long-term climate variations and are minimum values (*19*). The homogeneous thermal structure of ice is an advantage when the heat flow density and the temperature history are to be reconstructed (*20*).

Histograms from the GRIP reconstruction (Fig. 3) show that temperatures at the Last Glacial Maximum (LGM) were 23 ± 2 K colder than at present (*21*). The temperatures at this time, 25 ka, reflect the cold temperatures seen on the measured temperature profile at a depth of 1200 to 2000 m. Alternative reconstructions of the ice thickness and accumulation rates all reproduce LGM temperatures within 2 K (*9, 10, 22, 23*). The cold Younger Dryas and the warm Bølling/Allerød periods (*24*) are not resolved in the inverse reconstruction. The temperature signals of these periods have been obliterated by thermal diffusion because of their short duration (*25*). After the termination of the glacial period, temperatures in our record increase steadily, reaching a period 2.5 K warmer than present during what is referred to as the Climatic Optimum (CO), at 8 to 5 ka. Following the CO, temperatures cool to a minimum of 0.5 K colder than the present at around 2 ka. The record implies that the medieval period around 1000 A.D. was 1 K warmer than present in Greenland. Two cold periods, at 1550 and 1850 A.D., are observed during the Little Ice Age (LIA) with temperatures 0.5 and 0.7 K below the present. After the LIA, temperatures reach a maximum around 1930 A.D.; temperatures have decreased during the last decades (*26*). The climate history for the most recent times is in agreement with direct measurements in the Arctic regions (*27*). The climate history for the last 500 years agrees with the general understanding of the climate in the Arctic region (*28*) and can be used to verify the temperature amplitudes. The results show that the temperatures in general have decreased since the CO and that no warming in Greenland is observed in the most recent decades.

As seen in Fig. 3, resolution decreases back

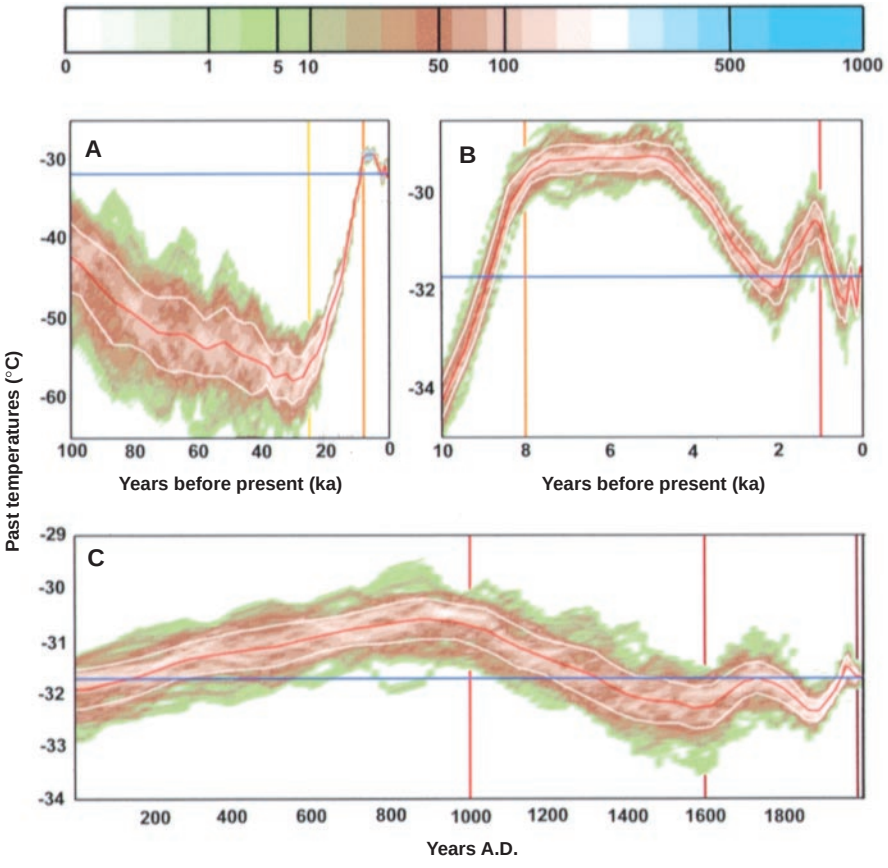


**Fig. 3.** The contour plots of all the GRIP temperature histograms as a function of time describes the reconstructed temperature history (red curve) and its uncertainty. The temperature history is the history at the present elevation (3240 m) of the summit of the Greenland Ice Sheet (*21*). The white curves are the standard deviations of the reconstruction (*18*). The present temperature is shown as a horizontal blue curve. The vertical colored bars mark the selected times for which the temperature histograms are shown in Fig. 2. (**A**) The last 100 ky BP. The LGM (25 ka) is seen to have been 23 K colder than the present temperature, and the temperatures are seen to rise directly into the warm CO 8 to 5 ka. (**B**) The last 10 ky BP. The CO is 2.5 K warmer than the present temperature, and at 5 ka the temperature slowly cools toward the cold temperatures found around 2 ka. (**C**) The last 2000 years. The medieval warming (1000 A.D.) is 1 K warmer than the present temperature, and the LIA is seen to have two minimums at 1500 and 1850 A.D. The LIA is followed by a temperature rise culminating around 1930 A.D. Temperature cools between 1940 and 1995.

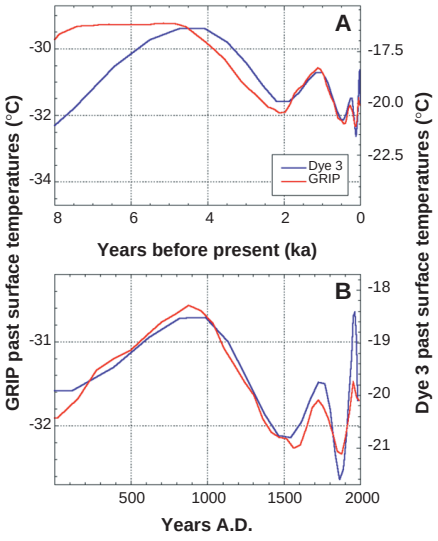


**Fig. 4.** The reconstructed temperature histories for GRIP (red curves) and Dye 3 (blue curves) are shown for the last 8 ky BP (**A**) and the last 2 ky BP (**B**). The two histories are nearly identical, with 50% larger amplitudes at Dye 3 than found at GRIP. The reconstructed climate must represent events that occur over Greenland, probably the high-latitude North Atlantic region.

in time (*25, 29*). For the GRIP reconstruction, an event with a duration of 50 years and an amplitude of 1 K can be resolved 150 years back in time with a measurement accuracy of 5 mK; an event with a similar amplitude but a duration of 1000 years can be detected back to 5 ka. An event that occurred 50 ka will now be observed in the temperature profile at the bedrock. Climate events for times older than 50,000 years before present (ky BP) are not well resolved (*30*). At Dye 3, the reconstructed climate history extends only to 7 ka, because the ice is 1000 m thinner than at the summit and surface accumulation rate is 50% higher. The LGM is not well resolved in the Dye 3 record, and consequently the geothermal heat flow density is not uniquely determined (*31*). On the other hand, the recent climate history has a higher resolution because of the increased accumulation (Fig. 4).

The Dye 3 record is nearly identical with the GRIP record back to 7 ka, but the amplitudes are 50% higher. Thus, the resolved climate changes have taken place on a regional scale; many are seen throughout the Northern Hemisphere (*27, 28, 32*). GRIP is located 865 km north of Dye 3 and is 730 m higher in elevation. Surface temperatures at the summit are influenced by maritime air coming in from the North Atlantic and air masses arriving from over northeastern Canada (associated with the Baffin trough) (*28, 32, 33*). Temperatures at Dye 3 will be influenced to a greater degree by the North Atlantic maritime air masses. Dye 3 is located closer to the center of the highest atmospheric variability, which is associated with large interseasonal, interannual, and decadal temperature changes (*32, 34*). It is therefore believed that the observed difference in amplitudes between the two sites is a result of their different geographic location in relation to variability of atmospheric circulation, even on the time scale of a millennium.

### References and Notes


1. Greenland Ice-Core Project (GRIP) members, *Nature* **364**, 203 (1993).
2. W. Dansgaard *et al.*, *ibid.*, p. 218.
3. N. S. Gundestup, D. Dahl-Jensen, S. J. Johnsen, A. Rossi, *Cold Reg. Sci. Technol.* **21**, 399 (1993).
4. G. D. Clow, R. W. Saltus, E. D. Waddington, *J. Glaciol.* **42**, 576 (1996).
5. The deep borehole is located in a building, and the liquid surface in the borehole is found at a depth of 40 m. The temperatures measured in the top 40 m are very disturbed, so we used measurements from an air-filled shallow borehole (100 m) near the borehole.
6. N. S. Gundestrup and B. L. Hansen, *J. Glaciol.* **30**, 282 (1984).
7. D. Dahl-Jensen and S. J. Johnsen, *Nature* **320**, 250 (1986).
8. D. Dahl-Jensen *et al.*, *J. Glaciol.* **43**, 300 (1997).
9. Between 50 and 20 ka, the ice thickness was 50 m less than at present, even though the ice sheet covered a larger area. The maximum ice thickness of 3230 m is found at 10 ka, after which the ice thickness gradually has decreased to the present 3028.6 m. The depression and uplift of the bedrock influences the elevation of the surface [S. J. Johnsen, D. Dahl-Jensen, W. Dansgaard, N. S. Gundestrup, *Tellus B* **47**, 624 (1995)].
10. K. M. Cuffey and G. D. Clow, *J. Geophys. Res.* **102**, 26383 (1997).
11. The past accumulation rates are determined by coupling them to the past (unknown) temperature through the relation $\lambda(T) = \lambda_O \exp[0.0467(T - T_O) - 0.000227(T - T_O)^2]$, where $\lambda(T)$ is the accumulation rate at the surface temperature $T$, $\lambda_O$ is the present ice accumulation rate, which is 0.23 m/year at GRIP and 0.49 m/year at Dye 3, and $T_O$ is the present surface temperatures at the sites: –31.7°C at GRIP and –20.1°C at Dye 3, respectively (*9*).
12. S. J. Johnsen, *IAHS-AISH Publ.* **118**, 388 (1977).
13. S. J. Johnsen and W. Dansgaard, *NATO ASI Ser. I Global Environ. Change* **2**, 13 (1992).
14. K. Mosegaard and A. Tarantola, *J. Geophys. Res.* **100**, 12431 (1995).
15. K. Mosegaard, *Inverse Problems* **14**, 405 (1998).
16. Our Monte Carlo scheme is a random walk in the high dimensional space of all possible models, m (temperature histories and geothermal heat flow densities). The temperature history has been divided in 125 intervals (interval length is 25 ky at 450 ka and 10 years at present). Including the geothermal heat flow density as an unknown the model space is 126-dimensional. In each step of the random walk, a perturbed model, $m^i_{pert}$ of the current model vector $m^i$ is proposed. The next model becomes equal to $m^i_{pert}$ with an acceptance probability $P_{accept} = \min\{1,\exp(-[S(m^i_{pert}) - S(m^i)])\}$, where $S(m) = \sum_j (g^j(m) - d^j_{obs})^2$, which is the misfit function measuring the difference between $g(m)$, the calculated borehole temperatures, and $d_{obs}$, the observed temperatures. If the perturbated model is rejected, the next model becomes equal to $m^i$ and a new perturbed model is proposed. To ensure an efficient sampling of all possible models, we developed ways of choosing the temperature histories and geothermal heat flow densities to be tested. The main scheme to perturb the models is to randomly select one of the 126 temperature/heat flow density parameters and change its value to a new value chosen uniformly at random within a given interval. A singular value decomposition (SVD) of the matrix $G = \{\partial g_j/\partial m_i\}$, evaluated in a near-optimal model, yields a set of eigenvectors in the model space whose orientations reveal efficient directions of perturbation for the random walk. The SVD method is included as a possible method of perturbing models especially in the start of the process as it speeds the Monte Carlo scheme significantly.
17. Of the $3.3 \times 10^6$ models tested during the random walk 30% have been accepted by the Monte Carlo scheme (*16*). Every 500 is chosen of those where the misfit function S (*16*) is less than the variance of the observations. The waiting time of 500 has been chosen to exceed the maximum correlation length of the output model parameters. This is a necessary condition for the 2000 models to be uncorrelated. To further ensure that the output models were uncorrelated, the random walk was frequently restarted at several random selected points in the model space.
18. The probabilistic formulation of the inverse problem leads to definition of a probability distribution in the model space, describing the likelihood of possible temperature histories and geothermal heat flow densities. The Monte Carlo scheme is constructed to sample according to this probability distribution. The histograms in Fig. 2 describe the probability distribution of the geothermal heat flow density and temperatures at times before present. The maxima in the histograms thus describe the most likely values. The method does not constrain the distributions to have a single maximum, indeed there could be histograms with several maxima, reflecting that more than one value of the temperature at this time would give a good fit to the observed temperature in the borehole. The histograms however, are all seen to have a well-defined zone with most likely past temperatures. A soft curve is fitted to the histograms and the maximum value is taken as the most likely value. The standard deviations shown in Fig. 3 are derived as deviations from the maximum value.
19. J. H. Sass, B. L. Nielsen, H. A. Wollenberg, R. J. Munroe, *J. Geophys. Res.* **77**, 6435 (1972).
20. C. Clauser *et al.*, *ibid.* **102**, 18417 (1997); L. Guillou-Frottier, J.-C. Marescal, J. Musset, *ibid.* **103**, 7385 (1998); H. N. Pollack, S. J. Hurter, J. R. Johnson, *Rev. Geophys.* **31**, 267 (1993); W. G. Powell, D. S. Chapman, N. Balling, A. E. Beck, in *Handbook of Terrestrial Heat-Flow Density Determination* (Kluwer Academic, New York, 1988), pp. 167–222.
21. In order to produce a past temperature record from the calculated past surface temperatures, the temperatures have been corrected to the present elevation of the GRIP site (and Dye 3 site respectively) using the surface elevation changes described in (*9*) and a lapse rate of 0.006 K/m.
22. K. M. Cuffey *et al.*, *Science* **270**, 455 (1995).
23. D. Dahl-Jensen, in *Proceedings of the Interdisciplinary Inversion Workshop 2*, Copenhagen, 19 May 1993, K. Mosegaard, Ed. (The Niels Bohr Institute for Astronomy, Physics and Geophysics, University of Copenhagen, Copenhagen, 1993), pp. 11–14.
24. C. U. Hammer *et al.*, *Report on the stratigraphic dating of the GRIP Ice Core. Special Report of the Geophysical Department* (Niels Bohrs Institute for Astronomy, Physics and Geophysics, University of Copenhagen, Copenhagen, in press).
25. J. Firestone, *J. Glaciol.* **41**, 39 (1995).
26. The amplitude of the warming at 1930 A.D. must be considered to be more uncertain. The information leading to this result are the measured temperatures in an open shallow borehole, where air movements could influence the measurements.
27. D. Fisher *et al.*, *NATO ASI Ser. I Global Environ. Change* **41**, 297 (1996); J. W. C. White *et al.*, *J. Geophys. Res.* **102**, 26425 (1997); J. W. Hurrel, *Science* **269**, 676 (1995); P. Frich *et al.*, in *DMI Scientific Report 96-1* (Danish Meteorological Institute, Copenhagen, 1996).
28. R. G. Barry and R. J. Charley, *Atmosphere, Weather & Climate* (Routledge, London, ed. 6, 1992); J. Overpeck *et al.*, *Science* **278**, 1251 (1997); H. H. Lamb, *Climate History and the Modern World* (Routledge, London, ed. 2, 1995); N. W. T. Brink and A. Weidick, *Quat. Res.* **4**, 429 (1974).
29. G. D. Clow, *Palaeogeogr. Palaeoclimatol. Palaeoecol.* **98**, 81 (1992).
30. To comply with this resolution the time steps have been chosen with increasing length back in time. The increasing length of the time steps can be considered as an efficient way of calculating the mean temperatures in the intervals so full available resolution is kept but the calculations are rationalized.
31. In (*7*), it is argued that parameter combinations of mean glacial temperature, mean glacial accumulation, and geothermal heat flow density can be found that fit the Dye 3 measurements due to the reduced resolution of the climate history reaching further back than 7 ka. A combination with a geothermal heat flow density of 38.7 mW/m$^2$ was chosen corresponding to a mean glacial temperature 12 K colder than the present temperatures. If a value of 51 mW/m$^2$ is chosen as that found for our inversion, the mean glacial temperature is 19 K colder than the present, which is well in agreement with the results found for the GRIP reconstruction. Comparison of the Dye 3 temperature history presented in (*7*) and that presented here shows a general good agreement for the last 7 ky. The history presented in (*7*) is more intuitive and less detailed, and the history has not been corrected for elevation changes. The ice thickness was assumed constant in this reconstruction.
32. L. K. Barlov, J. C. Rogers, M. C. Serreze, R. C. Barry, *J. Geophys. Res.* **102**, 26333 (1997).
33. R. A. Keen, *Occas. Pap. 34* (Institute of Arctic and Alpine Research, University of Colorado, Boulder, 1980).
34. S. Shubert, W. Higgins, C. K. Park, S. Moorthi, M. Svarez, *An Atlas of ECMWF Analyses (1980–87)*. Part II: *Second Moment Quantities*, *NASA Tech. Memorandum 100762* (1990); F. Rex, *World Surv. Climatol.* **4**, 1 (1969).


35. This is a contribution to the Greenland Ice Core Project (GRIP), a European Science Foundation program with eight nations and the European Economic Commission collaborating to drill through the central part of the Greenland Ice Sheet. G.D.C. thanks the USGS Climate History Program and NSF for support.

16 June 1998; accepted 1 September 1998